Revealing and controlling nuclear dynamics following inner-shell photoionization of N_2

Qingli Jing,[1,2,*] Hong Qian,[1,2] and Peng Xu[3]

[1]*Department of Optoelectronic Information of Science and Engineering, School of Science, Jiangsu University of Science and Technology, Zhenjiang 212003, China*

[2]*Applied Optics Research Center, School of Science, Jiangsu University of Science and Technology, Zhenjiang 212003, China*

[3]*Institute of Quantum Information and Technology, Nanjing University of Posts and Telecommunications, Nanjing, Jiangsu 210003, China*

(Received 1 August 2022; accepted 14 September 2022; published 29 September 2022)

In this paper, we apply the Monte Carlo wave packet method to study the ultrafast nuclear dynamics following inner-shell photoionization of N_2 exposed to an ultrashort intense x-ray pulse. The intermediate states in N_2^+ are highly excited so that autoionization takes place from these states to the quasibound or dissociative electronic states in N_2^{++}. The nuclear kinetic energy release (KER) spectra following double ionization of N_2 are obtained by using the spectral methods. The very sharp peaks in the nuclear KER spectra, which were, however, absent from many relevant experiments due to a limited vibrational resolution, can be ascribed to the long-lived vibrational resonances supported by the quasibound states in N_2^{++}. The origins for the other main characteristic structures appearing in the nuclear KER spectra are also identified. To control the fragmentation dynamics of doubly ionized N_2, the x-ray-pump–infrared-probe setting is employed. It is found that the laser-induced one-photon resonant transitions between the dissociative $1^1\Pi_g$ state and the quasibound $1^1\Pi_u$ state at around $R = 3$ a.u. are responsible for suppression or enhancement of the signals at different energy regions in the nuclear KER spectra. In addition, the delay-dependent nuclear KER distributions are constructed to achieve time-resolved imaging and controlling of the ultrafast nuclear dynamics that takes place following inner-shell photoionization of N_2.

DOI: 10.1103/PhysRevA.106.033122

I. INTRODUCTION

Probing the ultrafast dynamics in molecules has attracted a great deal of research interest due to the great advances in ultrafast laser technology and spectroscopy [1,2]. On the one hand, it is still challenging to interpret the ultrafast dynamics from the experimental observations since both the electronic and nuclear degrees of freedom are involved in molecules. On the other hand, considering the nuclear degrees of freedom makes simulation of strong field ionization of molecules, even for the diatomic molecules, very complicated, time-consuming, and resource-intensive. Despite the difficulty, the laser-induced dissociation and ionization dynamics of diatomic molecules such as H_2 [3–5], O_2 [6–8], and CO [9–13], has so far been investigated both experimentally and theoretically to reveal the physical mechanisms governing the ultrafast dynamics involved. To measure and obtain the lifetime for excited molecules, there are also studies of the relaxation dynamics in molecules interacting with high-energy extreme ultraviolet (XUV) or x-ray pulses. For example, due to the electron correlation effect, autoionization from doubly excited states [14–17] and Auger decay from highly excited states [18–21] can take place in molecules. For the latter case, inner-shell photoionization of molecules is subsequently followed by Auger decay, which eventually leaves the molecules doubly ionized.

With respect to double or multiple ionization of molecules, the Coulomb explosion imaging technique has been widely applied to identify and map out the electronic or nuclear dynamics involved [22–25]. Unlike the simplest case of H_2, molecular nitrogen—the most abundant molecule in the Earth's atmosphere—can exhibit new characteristics for its nuclear dynamics since the metastable states in the dicationic state of N_2 can support long-lived vibrational resonances. There have been considerable research efforts pouring into studying the double ionization process of N_2 [25–34]. When particular attention is given to the nuclear dynamics, the nuclear kinetic energy release (KER) spectra following dissociative ionization of N_2 have been measured by different experimental settings, where the infrared (IR), XUV, or x-ray pulses were applied [16,35–38].

This paper is mainly inspired and motivated by the earlier works on the molecular nitrogen in x-ray-pump–IR-probe settings [16,32–34]. The time-resolved pump-probe experiments at the LCLS reported an enhancement of fragmented N_2^{++} yield due to strong field-induced dissociation [32]. This enhancement was later confirmed and discussed by authors of two theoretical works where a systematic study for controlling over the Coulomb explosion imaging of N_2^{++} was carried out through the quantum dynamics calculations [33] and the fewest switches surface hopping method [34]. Other than the Auger electron energy spectra and the yields of bound N_2^{++} fragments at different Auger energies in Refs. [33,34], we are concerned with uncovering the nuclear dynamics from the nuclear KER spectra following inner-shell ionization of N_2.

*jingqingli@yeah.net

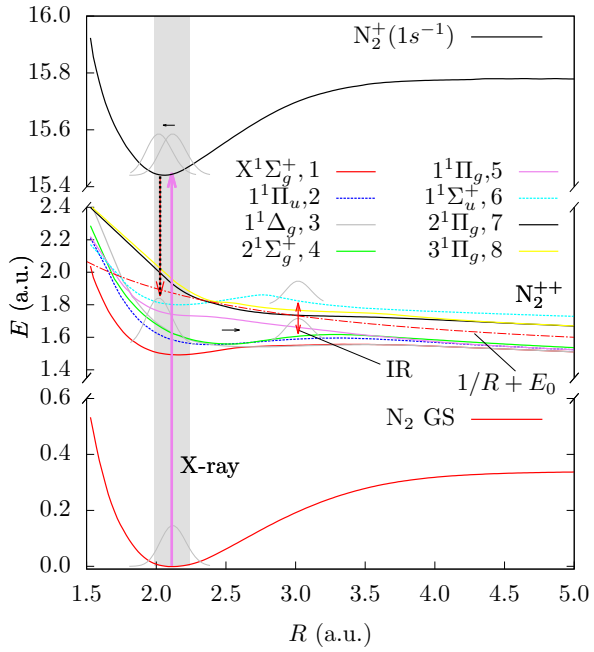

FIG. 1. Potential energy curves involved in the double ionization process of N_2 as a function of the internuclear distance R. From bottom to top, at around $R = 2.1$ a.u., the curves are for the ground state of N_2, eight selected states of ungerade and gerade symmetries in $N_2{}^{++}$, and the intermediate state in $N_2{}^+(1s^{-1})$, respectively. These curves are directly extracted from Fig. 2 in Ref. [33], where they are obtained by the complete-active-space self-consistent-field theory. To show the potential curves for the eight states in $N_2{}^{++}$ are parallel to the $1/R$ curve at large internuclear distances, the $E_0 + 1/R$ curve is also plotted. The Franck-Condon region is indicated by a gray shaded area.

Due to the absence of the corresponding nuclear KER spectra in the previous works, we apply the Monte Carlo wave packet (MCWP) approach to simulate double ionization of N_2 in this paper. This method has been proven to be especially useful in reproducing the nuclear KER spectra following double ionization of diatomic molecules such as H_2 [39–43] and O_2 [44]. We will show that the nuclear KER spectra obtained in this paper can offer clear evidence for laser-induced couplings between states in $N_2{}^{++}$ and thus can provide deeper insight into the ultrafast dynamics of interest.

This paper is organized as follows. We first introduce the process considered in this paper in Sec. II. Then the implementation of the MCWP approach to simulate double ionization of N_2 is described in Sec. III. In Sec. IV, we present the simulation results obtained from two spectral methods and the corresponding discussions of the nuclear KER spectra following autoionization of $N_2{}^+$ in different pulse settings. Section V concludes. Throughout this paper, atomic units (a.u.) are used unless stated otherwise.

II. PROCESS

In this paper, we study the double ionization process of N_2 illustrated in Fig. 1. The N_2 molecule is initially in its ground electronic and vibrational state. Through interaction with an intense x-ray pulse, a $1s$ electron is removed from one of the nitrogen atoms in N_2 and suddenly launches the nuclear wave packets evolving slowly along the potential energy curves for the highly excited electronic states in the core-ionized $N_2{}^+$. The potential energy curves for these states of gerade and ungerade symmetries are almost parallel to each other. For simplicity, we only involve the first state of ungerade symmetry in our simulation. Due to the electron correlation effect, subsequent autoionization from this unstable state can take place, resulting in the nuclear wave packets evolving along the potential energy curves for the electronic states in $N_2{}^{++}$. It was reported experimentally that the partial autoionization rates from the inner-shell ionized $N_2{}^+$ were dependent on the target states in $N_2{}^{++}$ [33,45], and the total autoionization rate Γ_A was around 103 meV/$\hbar$ (0.0038 a.u.) [46], which corresponds to a lifetime of $1/\Gamma_A = 6.4$ fs. If only one x-ray pulse is applied, the final nuclear KER spectrum can be obtained from the nuclear wave packets at the time instants when autoionization of $N_2{}^+$ takes place. If a femtosecond probe pulse is also applied, the electric dipole operator can only connect states of opposite parity according to the selection rules for the electric dipole transitions in the case of homonuclear diatomic molecules. Therefore, strong transitions can be allowed between the electronic states of gerade and ungerade symmetries in $N_2{}^{++}$. In fact, the selection rules also impose some further restrictions: The transitions are allowed with $\Delta S = 0$, $\Delta\Lambda = 0, \pm 1$, and $\Delta J = 0, \pm 1$, where S, Λ, and J are the quantum numbers for the total spin, the projection of the electronic orbital angular momentum along the internuclear axis, and the total angular momentum, respectively. In addition, the laser-induced dipole transitions become significantly reduced when the states are energetically well separated with respect to the IR photon energy. When an IR pulse is present, we shall obtain the nuclear KER spectrum for double ionization of N_2 from the nuclear wave packets in $N_2{}^{++}$ after the IR pulse is switched off. The nuclear KER spectra are capable of showing the effect of the IR pulse on the nuclear dynamics following autoionization of $N_2{}^+$.

III. METHOD

In this paper, we apply the MCWP approach to study the double ionization process of N_2 outlined in Sec. II. The implementation and validation of this method in simulating double ionization of diatomic molecules have been discussed in detail elsewhere in Refs. [40–43]. To summarize, this method adopts a non-Hermitian Hamiltonian to describe ionization of a molecular system as a decay process, i.e.,

$$H = H_s - \frac{i}{2}\sum_{mn} C_{mn}{}^{+} C_{mn}. \tag{1}$$

The Hermitian system Hamiltonian H_s in Eq. (1) is a superposition of three parts, i.e., $H_s = T_N + H_e + V_I(t)$. T_N is the nuclear kinetic energy operator, H_e is the field-free electronic Hamiltonian, and $V_I(t) = -\vec{\mu}\cdot\vec{F}(t)$ is the light-molecule interaction potential, with μ the transition dipole moment operator and $\vec{F}(t)$ the electric field component of the applied laser pulse. Here, C_{mn} in the non-Hermitian term of Eq. (1) is a jump operator that specifies the transition pathway from the electronic state $|\phi^e_{R,m}\rangle$ in the molecular system of

concern to the electronic state $|\phi^{e-1}_{R,n}\rangle$ in the system with one electron less. For the case of incoherent transitions, $C_{mn} = \int d\vec{R}\sqrt{\Gamma_{mn}(\vec{R},t)}|\phi^{e-1}_{R,n}\rangle\langle\phi^{e}_{R,m}| \otimes |\vec{R}\rangle\langle\vec{R}|$, where $|\vec{R}\rangle$ is the position eigenket for the nuclear coordinate $\vec{R}$, and $\Gamma_{mn}(\vec{R},t)$ is the ionization (photoionization or autoionization) rate from the $|\phi^{e}_{R,m}\rangle$ state to the $|\phi^{e-1}_{R,n}\rangle$ state. Here, m and n are positive integers numbering the states in each charge state, e.g., if $m = 1$ and $n = 1$, the operator C_{11} induces a quantum jump occurring between the lowest electronic states in two charge states.

To obtain the nuclear dynamics in a given molecular system where the Born-Oppenheimer approximation is valid, we solve the time-dependent Schrödinger equation (TDSE) for the Hamiltonian in Eq. (1) by expressing the total wave function with the ansatz:

$$|\Psi(t)\rangle = \sum_m |\chi_m(t)\rangle \otimes |\phi^{e}_{R,m}\rangle. \tag{2}$$

Here, $|\phi^{e}_{R,m}\rangle$ is the electronic eigenstate satisfying the time-independent Schrödinger equation for the electronic Hamiltonian, i.e., $H_e|\phi^{e}_{R,m}\rangle = E_m(\vec{R})|\phi^{e}_{R,m}\rangle$, with $E_m(\vec{R})$ the potential energy surface for the $|\phi^{e}_{R,m}\rangle$ state. Here, $|\chi_m(t)\rangle$ is the state vector for the nuclei when the molecule is in the $|\phi^{e}_{R,m}\rangle$ state. In the MCWP method, the total wave function of a molecule at a given charge state is a coherent superposition of the bound electronic states involved in the process.

Substituting the total wave function into the TDSE and projecting both sides of the TDSE on the eigenbra $\langle\phi^{e}_{R,m}|\langle\vec{R}|$, we get the evolution equation for the nuclear wave function $\chi_m(\vec{R},t) = \langle\vec{R}|\chi_m(t)\rangle$ in the $|\phi^{e}_{R,m}\rangle$ state:

$$i\dot{\chi}_m(\vec{R},t) = \left[T_N + E_m(\vec{R}) - \frac{i}{2}\sum_n \Gamma_{mn}(\vec{R},t)\right] \times \chi_m(\vec{R},t) + \sum_{k\neq m} V_{mk}(\vec{R},t)\chi_k(\vec{R},t), \tag{3}$$

with $V_{mk}(\vec{R},t) = \langle\phi^{e}_{R,m}|V_I(t)|\phi^{e}_{R,k}\rangle = \langle\phi^{e}_{R,m}|\vec{\mu}|\phi^{e}_{R,k}\rangle\cdot\vec{F}(t) = \vec{D}_{mk}(\vec{R})\cdot\vec{F}(t)$. Here, $\vec{D}_{mk}(\vec{R})$ is the dipole moment function between the $|\phi^{e}_{R,m}\rangle$ and $|\phi^{e}_{R,k}\rangle$ states. Note that, due to the non-Hermitian term in Eq. (1), the eigenenergy for a given electronic state becomes complex in Eq. (3), i.e., $\tilde{E}_m(\vec{R}) = E_m(\vec{R}) - i/2\sum_n \Gamma_{mn}(\vec{R},t)$. For the highly excited state in N_2^+, the imaginary part of its complex energy is $-\Gamma_A/2$, with Γ_A the autoionzation rate of the core-ionized N_2^+. In this paper, the applied x-ray and IR pulses are linearly polarized, and their polarization directions are parallel to the molecular axis. The molecule to be studied is assumed to be rotationally frozen; therefore, Eq. (3) can be reduced to a one-dimensional equation that is much easier to solve by replacing the vector $\vec{R}$ with the scalar R. This is a good approximation since the natural timescale for rotation of a molecule is usually much larger than that for vibration of the same molecule. We solve the simplified Eq. (3) by using the split-operator fast Fourier transform method [47], and the dipole moment functions $D_{mk}(R)$ between the electronic states in N_2^{++} are taken from Ref. [33].

When applying the MCWP approach to simulate double ionization of N_2, one strategy is to solve Eq. (3) in the charge state of N_2, N_2^+, or N_2^{++}, with the stochastic occurrence of quantum jumps. Such a full-time evolution of the nuclear wave packets from N_2 is a stochastic trajectory. According to the number of jumps, there are three categories of trajectories: Trajectories without any jump lead to neutral N_2 fragments; trajectories with one jump lead to single charged N_2^+ fragments; and trajectories with two jumps lead to doubly charged N_2^{++} fragments. The more detailed execution of this stochastic sampling strategy can be found in Ref. [48]. To obtain results that capture real physics, we have to include as many trajectories as possible. To greatly reduce the computational costs, we use the deterministic sampling method instead to pick up trajectories with two quantum jumps. This sampling method was confirmed to perform well in earlier works [40–43]. In this case, we solve Eq. (3) in each charge state, and the jump operator determines the initial nuclear wave packet in the new charge state. Suppose the jump takes place at t from the $|\phi^{e}_{R,m}\rangle$ state to the $|\phi^{e-1}_{R,n}\rangle$ state; then the initial total wave function in the new charge state at the next time step is $|\Psi(t+\Delta t)\rangle = \frac{C_{mn}|\Psi(t)\rangle}{\langle\Psi(t)|C^+_{mn}C_{mn}|\Psi(t)\rangle}$. Correspondingly, the initial nuclear wave packet in this charge state is $\chi_n(R,t+\Delta t) = \langle\phi^{e-1}_{R,n}|\Psi(t+\Delta t)\rangle$. The probability of each trajectory is related to the ionization probabilities at the first and second jump times t_1 and t_2 ($t_2 > t_1$). The nuclear KER spectrum shows the yield of the two N^+ fragments at different total kinetic energies. For a given trajectory, it is extracted from the final nuclear wave packet $\chi_m^{N_2^{++}}(R,t_e)$ in N_2^{++}:

$$P_{E,mk}(t_2;t_1) = \left|\int dR K_E(R)\chi_m^{N_2^{++}}(R,t_e)\right|^2. \tag{4}$$

Here, $\chi_m^{N_2^{++}}(R,t_e)$ depends implicitly on the first and second jump times. It is the nuclear wave packet in the $|\phi^{N_2^{++}}_{R,m}\rangle$ state in N_2^{++} at the time instant of t_e. In general, for N_2 interacting with a single x-ray pulse, t_e is the second jump time t_2; when there is an additional IR pulse inducing a large coupling between the electronic states in N_2^{++}, t_e is the end of the IR pulse. We see from Fig. 1 that the potential energy curves for the electronic states in N_2^{++} are not purely dissociative, and thus, some metastable N_2^{++} fragments are long-lived. In Eq. (4), $K_E(R)$ specifies either the eigenstates of the potential energy curves for the electronic states in N_2^{++} or the energy-normalized Coulomb wave functions for the $1/R$ curve. These two options correspond to the two spectral methods applied to obtain the nuclear KER spectra in the following section. The nuclear KER spectrum following double ionization of N_2 is then obtained by a weighted sum of the KER spectra for a large amount of deterministic trajectories, i.e.,

$$P_E = \sum_{m,n,t_1,k,t_2} P_1(t_1)P_{1mn}(t_1)P_2(t_2;t_1)P_{2k}(t_2;t_1) \times P_{E,mk}(t_2;t_1). \tag{5}$$

For a given trajectory, $P_1(t_1) = \frac{dP(t)}{dt}|_{t=t_1}$ is the probability for the first jump taking place at t_1, where $P(t)$ is the monotonically decreasing probability staying in N_2 due to photoionization induced by the x-ray pulse. It is closely related to the optical parameters of the applied x-ray pulse. For example, for N_2 interacting with a 4-fs sine-square x-ray pulse with a photon energy of 15.44 a.u., the photoionization

cross-section at this photon energy is ∼0.1 a.u. [49], and the total ionization probability for a N_2 molecule is $P(t = 4\ \text{fs}) - P(t = 0) = 0.0063$ when the peak field strength is 0.05338 a.u. When there is more than one state in either N_2 or N_2^+, the first ionization events can take place via several ionization channels. The probability for each ionization channel is $P_{1mn}(t_1) = \frac{\langle\Psi(t_1)|C_{mn}{}^+C_{mn}|\Psi(t_1)\rangle}{\sum_{mn}\langle\Psi(t_1)|C_{mn}{}^+C_{mn}|\Psi(t_1)\rangle}$, with $|\Psi(t_1)\rangle$ the total wave function in N_2 at the time step when the first ionization occurs. In our simulation, we involve one state in both N_2 and N_2^+; thus, there is only one ionization channel from N_2 to N_2^+, i.e., $m = 1$ and $n = 1$, and we have $P_{111}(t_1) = 1$. Once the first jump occurs, the system evolves in N_2^+ until the second jump, i.e., autoionization, takes place. Here, $P_2(t_2; t_1)$ is the conditional probability for the second jump event taking place at t_2, when the first jump occurs at t_1. It has a similar form with P_1, i.e., $P_2(t) = \frac{dP(t)}{dt}|_{t=t_2}$, and the only difference is that $P(t)$ here is the monotonically decreasing probability staying in N_2^+. Similarly, the eight states in N_2^{++} indicate that there are eight autoionization channels and $P_{2k}(t_2; t_1) = \frac{\langle\Psi(t_2)|C_{1k}{}^+C_{1k}|\Psi(t_2)\rangle}{\sum_k\langle\Psi(t_2)|C_{1k}{}^+C_{1k}|\Psi(t_2)\rangle}$, with $k = 1, 2, 3..., 8$ specifies the probability for each individual second ionization channel, with $|\Psi(t_2)\rangle$ the total wave function in N_2^+ at the time step when the second ionization occurs. According to the calculated state-resolved Auger yields in Ref. [33], the relative probabilities P_{2k} for the individual channels with the initial states in N_2^{++} corresponding to the $2^1\Sigma_g{}^+$, $1^1\Delta_g$, $1^1\Sigma_u{}^+$, $1^1\Pi_g$, $1^1\Pi_u$, $X^1\Sigma_g{}^+$, $2^1\Pi_g$, and $3^1\Pi_g$ states are 0.412, 0.204, 0.145, 0.119, 0.074, 0.046, 0, and 0, respectively.

To obtain the nuclear KER spectrum that captures real physics, we manage to minimize the unphysical reflections of the nuclear wave packets from the boundaries by increasing the simulation box size to avoid the use of the complex absorbing boundaries. The total propagation time t_T varies on a case-by-case basis, which depends on the autoionization rates, the pump-probe delay, the pulse duration, and the spectral methods applied. In this paper, the simulation box extends from $R_{\text{min}} = 1.5$ a.u. to $R_{\text{max}} = 45.4$ a.u. Meanwhile, to ensure convergence of the final results, the spatial step is chosen to be $\Delta R = 0.0214$ a.u. and the time step to be $\Delta t = 1$ a.u. The computational costs also depend on the sampling densities for the first and second jumps.

In the ideal case, the trajectories are launched when the first jumps take every time step during the x-ray pulse, and the second jumps take every time step after the first jumps. However, such a huge amount of trajectories mean unaffordable time and resource consumption. To reduce the number of trajectories to an acceptable level, we assume the first jump to take place at the time instant of the maximum of the temporal intensity profile of the x-ray pulse. This is a reasonable treatment since the applied x-ray pulse is very short, and by doing so, we have included the trajectories with the largest ionization probabilities in the first jump. For x-ray pulses with relatively large pulse durations, this assumption is not valid, and more first jumps should be included. The second jumps are assumed to occur every 50 time steps after the first jump takes place. For the core-ionized N_2^+, the probability of survival is 0.368 after its lifetime of 6.4 fs, and it takes ∼1500 a.u. (36.6 fs) to almost totally decay to N_2^{++} with the probability of survival being ∼0.0034. Thus, to include the dominant trajectories, there are $\sim 1500/50 = 30$ second jumps after the first jump, resulting in the launch of $\sim 8 \times 30 = 240$ trajectories in each simulation. We have verified such a great reduction of the number of trajectories can still capture well the main features of the nuclear KER spectra.

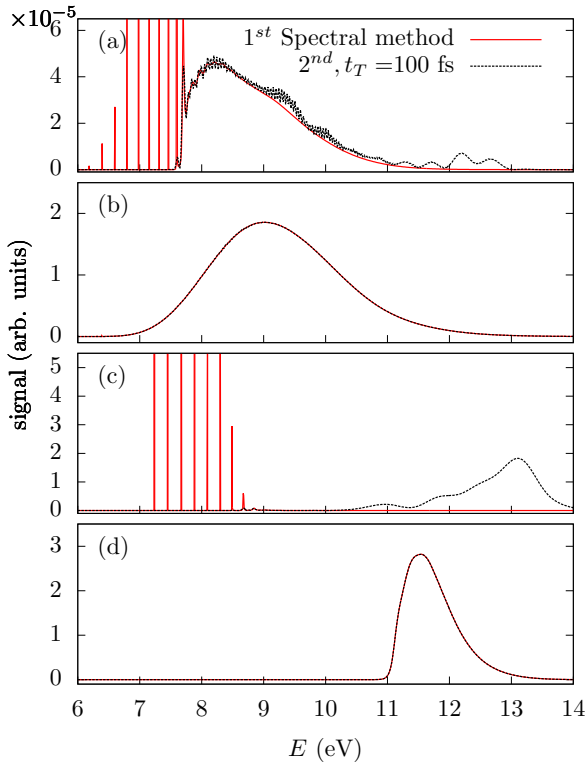

FIG. 2. State-resolved nuclear kinetic energy release (KER) spectra obtained by the two spectral methods following double ionization of N_2 interacting with a single x-ray pulse. Results for the dominant channels with the final states corresponding to the (a) $2^1\Sigma_g{}^+$, (b) $1^1\Delta_g$, (c) $1^1\Sigma_u{}^+$, and (d) $1^1\Pi_g$ states in N_2^{++}. Optical parameters for the x-ray pulse are as follows: $\omega_X = 15.44$ a.u., $\tau_X = 4$ fs, and $F_{X0} = 0.05338$ a.u. The total propagation time is $t_T = 100$ fs.

IV. RESULTS AND DISCUSSIONS

In this section, the simulation results from the MCWP method for the process described in Sec. II are presented and analyzed.

A. N_2 interacting with a single x-ray pulse

We first present the state-resolved nuclear KER spectra for the dominant autoionization channels following photoionization of N_2 through interacting with an x-ray pulse in Fig. 2. The x-ray pulse has a sine-square envelope, and its nonzero temporal field distribution satisfies $F_X(t) = F_{X0}\sin^2(\frac{\pi t}{\tau_X})\cos(\omega_X t)$, $0 \leqslant t \leqslant \tau_X$. In this paper, the optical parameters of the x-ray pulse are as follows: The photon energy is $\omega_X = 15.44$ a.u., the pulse duration is $\tau_X = 4$ fs, and the peak field strength is $F_{X0} = 0.05338$ a.u. We assume the photoionization cross-section of N_2 at the x-ray photon energy is $\sigma_X = 0.1$ a.u., which is comparable with the result

in Ref. [49]. The corresponding photoionization rate takes the form of $\Gamma_X(t) = \frac{I_X(t)\sigma_X}{\hbar\omega_X}$, where $I_X(t)$ is the temporal intensity profile of the x-ray pulse. The four panels in Fig. 2 correspond to the contribution from the channels with the final states of $2^1\Sigma_g{}^+$, $1^1\Delta_g$, $1^1\Sigma_u{}^+$, and $1^1\Pi_g$ in $N_2{}^{++}$. In each panel, we first apply the spectral method to obtain the nuclear kinetic energy spectrum by projecting the final nuclear wave packet in $N_2{}^{++}$ on the eigenstates of the corresponding potential energy curve (the solid line). It is clear that, for the metastable states in Figs. 2(a) and 2(c), the allowed vibrational resonances appear as very sharp peaks at the low kinetic energy region, indicating relatively large lifetimes for these resonances. The long-lived $N_2{}^{++}$ fragments would eventually decay into two N^+ fragments. However, because of the limited vibrational resolution and measurement time in the experiments, authors of very few works witnessed the presence of such sharp vibrational resonances in the nuclear KER spectra.

To illustrate the properties of the vibrational resonances in each electronic state, we apply an alternative spectral method by projecting the final nuclear wave packets in $N_2{}^{++}$ on the Coulomb wave functions for the $1/R$ curve. It is a reasonable treatment since these potential energy curves in $N_2{}^{++}$ are almost parallel to the $1/R$ curve at internuclear distances $R \geqslant 4.5$ a.u., as we can see from Fig. 1. We show the corresponding results by the dashed lines in Fig. 2. We see that, if the potential energy curves are dissociative, the two spectral methods can provide very similar results, as shown in Figs. 2(b) and 2(d). If the potential energy curves are not purely dissociative, there are apparent discrepancies between the spectra obtained by the two methods. In fact, whether the spectrum from this spectral method reproduces well the spectrum from the other method has a close relationship with the total propagation time t_T. To better elucidate the influence of t_T, we present in Fig. 3 the results for the two metastable states $2^1\Sigma_g{}^+$ and $1^1\Sigma_u{}^+$ with t_T =100, 150, and 300 fs. It is clear that, for an increased propagation time, the difference between the results from the two methods is reduced, and the sharp resonances are gradually present and reproduced in the spectra obtained by the second spectral method. This means that different vibrational resonances have different lifetimes, and they take different times to tunnel through the barriers of their potential energy curves. For a measurement time that is not sufficient for the long-lived vibrational resonances to decay, we propose to use a combination of these two spectral methods to get the nuclear KER spectrum for the metastable state in $N_2{}^{++}$: Apply the first spectral method to obtain the high-energy part of the nuclear KER spectrum, and apply the second spectral method to obtain the remaining part of the nuclear KER spectrum. The boundary between the low- and high-energy regions of the nuclear KER spectrum is the high-energy limit for the vibrational resonances, which is indeed the dissociation energy from the top of the barrier to infinitely large internuclear distances of the potential energy curve.

Having demonstrated the applicability of the two spectral methods, now we apply them to obtain the nuclear KER spectra following double ionization of N_2 for a specific measurement time. We present in Fig. 4 the nuclear KER spectrum for N_2 interacting with the x-ray pulse mentioned above (the solid line) for t_T = 100 fs. We see that the spectrum has peaks at ∼7.3, 7.7, 8.2, and 11.5 eV, which reproduces the peaks

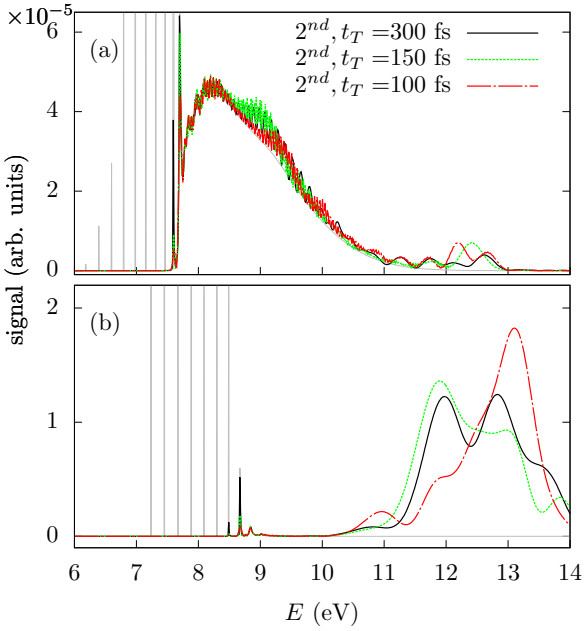

FIG. 3. State-resolved nuclear kinetic energy release (KER) spectra following double ionization of N_2 interacting with an x-ray pulse obtained by the second spectral method with t_T = 100, 150, and 300 fs. Results for the final states of (a) $2^1\Sigma_g{}^+$ and (b) $1^1\Sigma_u{}^+$ in $N_2{}^{++}$. The optical parameters for the x-ray pulse are identical to Fig. 2.

at ∼8 and 11 eV in the experiments [25,38]. To figure out the origins for these peaks, we also present the state-resolved spectra from individual channels of different final states in $N_2{}^{++}$ in Fig. 4 (the dashed lines). It is clear that the $1^1\Pi_u$ state in $N_2{}^{++}$ contributes most to the peak of 7.3 eV. The peak of 7.7 eV is mainly from the contribution of the $2^1\Sigma_g{}^+$ state. These two peaks are sharp and mainly come from tunneling decay of the vibrational resonances through the barriers of the potential energy curves. In addition, the $1^1\Pi_g$ state contributes most to the peak of 11.5 eV, which results from direct dissociation of the nuclear wave packets along the corresponding potential energy curve. The peak of 8.2 eV mainly comes from the $2^1\Sigma_g{}^+$ state. This peak is ascribed to the occurrence

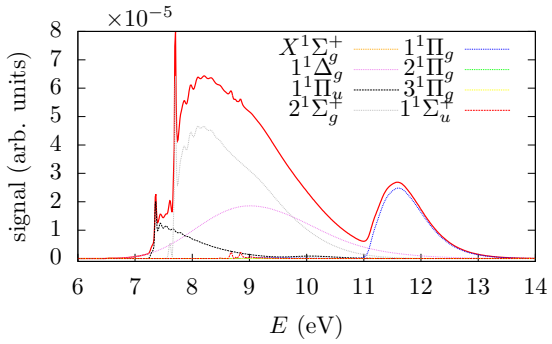

FIG. 4. Nuclear kinetic energy release (KER) spectra following double ionization of N_2 interacting with a single x-ray pulse (the solid line) obtained by the two spectral methods with t_T = 100 fs. The state-resolved spectra are also plotted (the dashed lines).

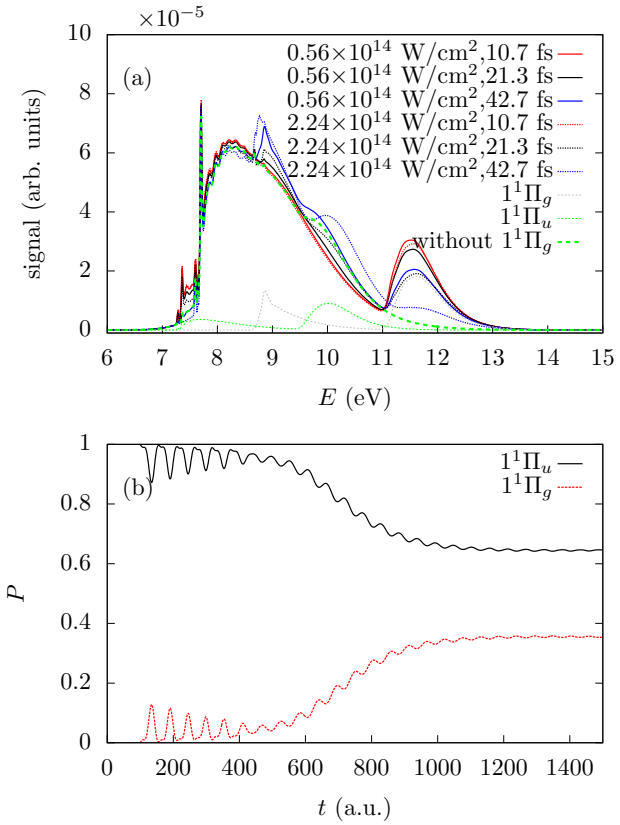

FIG. 5. (a) Nuclear kinetic energy release (KER) spectra following double ionization of N_2 in the x-ray-pump–infrared (IR)-probe configurations for $t_T = 150$ fs. The optical parameters for the IR pulses are as follows: The wavelength is 800 nm, the pump-probe delay is 0 fs, the peak intensity is either $I_0 = 2.24 \times 10^{14}$ W/cm^2 or $I_0 = 0.56 \times 10^{14}$ W/cm^2, and the full width at half maximum (FWHM) duration is $\tau_{IR} = 10.7$ fs (4 optical cycles), 21.3 fs (8 optical cycles), or 42.7 fs (16 optical cycles). The spectra of the $1^1\Pi_g$ state, of the $1^1\Pi_u$ state, and of the states without the $1^1\Pi_g$ state are also plotted for the case of $I_0 = 0.56 \times 10^{14}$ W/cm^2 and $\tau_{IR} = 42.7$ fs. (b) Time-dependent populations of the $1^1\Pi_g$ and $1^1\Pi_u$ states for a trajectory with $t_1 = 83$ a.u., $t_2 = 99$ a.u., and $1^1\Pi_u$ as the initial state in $N_2{}^{++}$ ($I_0 = 0.56 \times 10^{14}$ W/cm^2 and $\tau_{IR} = 42.7$ fs).

of over-the-barrier dissociation of the nuclear wave packets along the potential energy curve.

B. N_2 in the x-ray-pump–IR-probe configuration

For N_2 interacting with an x-ray pulse, as the x-ray photon energy is much larger than the energy gaps between the states in $N_2{}^{++}$, the interaction between the doubly charged $N_2{}^{++}$ and the remaining part of the x-ray pulse can be neglected. Authors of previous studies [16,32–34] have shown that the near-IR pulse can strongly couple the states in $N_2{}^{++}$ and thus dramatically influences the fragmentation dynamics of $N_2{}^{++}$. To explore the influence of the optical parameters of the IR pulse such as the peak intensity and the pulse duration on the nuclear dynamics, we present in Fig. 5 the nuclear KER spectra for N_2 in different x-ray-pump–IR-probe configurations with a pump-probe delay of $\tau = 0$ fs for $t_T = 150$ fs. The applied IR pulses have Gaussian envelopes, and the temporal electric fields satisfy $F_{IR}(t) = F_0 \exp[-(t - \tau_X/2 - \tau)^2/\tau_{IR}^2] \cos(\omega t)$. As an extended study, the optical parameters for the IR pulses are taken identical to Ref. [33]: The wavelength is $\lambda = 800$ nm, the peak intensity is 0.56×10^{14} W/cm^2 or 2.24×10^{14} W/cm^2, and the full width at half maximum (FWHM) duration is $\tau_{IR} = 10.7$ fs (4 optical cycles), 21.3 fs (8 optical cycles), or 42.7 fs (16 optical cycles), respectively.

We see in Fig. 5(a) that these spectra generally look similar except that the signals peaking at around $E = 7.5$ and 11.5 eV are suppressed, and the signals peaking at around $E = 9$ and 10 eV are enhanced for increasing the IR pulse duration or peak intensity. This effect is a manifestation of the laser-induced transitions between the states in $N_2{}^{++}$ and is more pronounced in a spectrum for a larger IR pulse duration or peak intensity. To illustrate the origin for the newly appeared peaks at ~9 eV, we also present in Fig. 5(a) the spectra of the $1^1\Pi_g$ state, of the $1^1\Pi_u$ state, and of the states other than the $1^1\Pi_g$ state for a given case: The duration of the IR pulse is 42.7 fs, and the peak intensity is 0.56×10^{14} W/cm^2. After a comparison with the state-resolved spectra in Fig. 4, we can conclude that the enhancement at ~9 eV and the suppression at ~7.5 eV reflect a net transition from the $1^1\Pi_u$ state to the $1^1\Pi_g$ state due to the one-photon resonance when the nuclear wave packet along the $1^1\Pi_u$ curve moves to the internuclear positions at around $R = 3$ a.u. This transition can be confirmed in Fig. 5(b) by the time-dependent populations of the $1^1\Pi_u$ and $1^1\Pi_g$ states for a given trajectory with $t_1 = 83$ a.u., $t_2 = 99$ a.u., and $1^1\Pi_u$ as the initial state in $N_2{}^{++}$. Thus, an IR pulse with a relatively larger pulse length or peak intensity can be applied to induce relatively larger transitions from the $1^1\Pi_u$ state to the $1^1\Pi_g$ state. These transitions result in a relatively smaller portion of the nuclear wave packet left in the inner barrier of the $1^1\Pi_u$ curve, and tunneling of the nuclear wave packet through this barrier is consequentially suppressed. In addition, the peak at ~10 eV in Fig. 5(a), which becomes more pronounced for longer and more intense IR pulses, comes directly from the $1^1\Pi_u$ state and indicates a net transition from the $1^1\Pi_g$ state to the $1^1\Pi_u$ state.

Finally, we are interested in investigating the influence of the pump-probe delay on the nuclear dynamics involved in the double ionization process of N_2. We first present the nuclear KER spectra with $t_T = 150$ fs in Fig. 6(a) for N_2 interacting with the x-ray and IR laser pulses for delays ranging from 0 to 60 fs. Here, a positive delay means the maximum of the temporal intensity envelope of the x-ray pulse arrives before that of the IR pulse. The optical parameters of the IR pulses are also identical to the pulse parameters in Ref. [33]: The wavelength is $\lambda = 800$ nm, the pulse duration is $\tau_{IR} = 10.7$ fs, and the peak intensity is 2.24×10^{14} W/cm^2. We can see that the spectra at most delays in Fig. 6(a) have similar structures, and the peaks at ~7.8, 8.2, and 11.5 eV in the delay-averaged nuclear KER spectrum in Fig. 6(b) have similar origins as the corresponding peaks in Fig. 4. Despite the overall similarity of the spectra in Fig. 6(a), we can still see that the spectra change dramatically when the delays are ~17 fs, where the signal peaking at ~11.5 eV is greatly suppressed and a peak at ~10 eV appears. This signature, as discussed in Fig. 4, comes from the enhanced transition from the $1^1\Pi_g$ state to the $1^1\Pi_u$ state due to the one-photon resonance at around $R = 3$

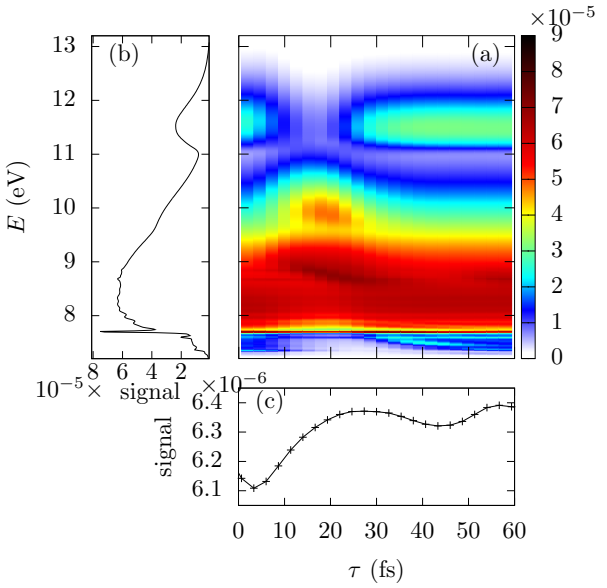

FIG. 6. (a) Nuclear kinetic energy release (KER) spectra with $t_T = 150$ fs following double ionization of N_2 as a function of the delay between the x-ray pump pulse and the infrared (IR) probe pulse. (b) Averaged nuclear KER spectrum for the spectra with delays between 0 and 60 fs. (c) Total yield for the fragmented N_2^{++} as a function of delay. The other optical parameters of the IR pulses are identical to Fig. 3.

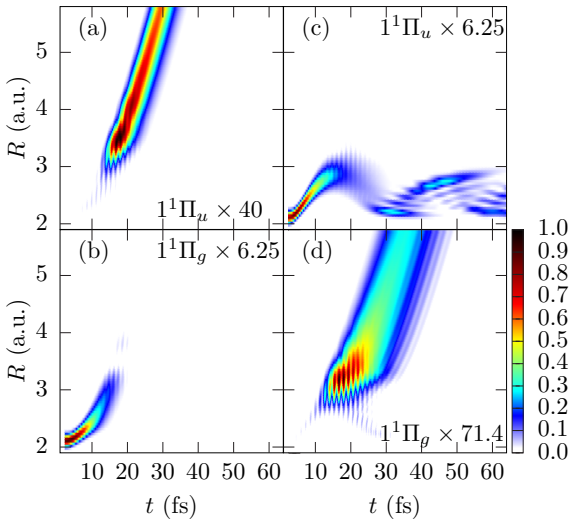

FIG. 7. The evolution of the nuclear wave packets along the (a) $1^1\Pi_u$ and (b) $1^1\Pi_g$ curves for the trajectory with selected parameters: $t_1 = 83$ a.u., $t_2 = 99$ a.u., and $1^1\Pi_g$ as the initial state in N_2^{++}; the evolution of the nuclear wave packets along the (c) $1^1\Pi_u$ and (d) $1^1\Pi_g$ curves for the trajectory with selected parameters: $t_1 = 83$ a.u., $t_2 = 99$ a.u., and $1^1\Pi_u$ as the initial state in N_2^{++}. The optical parameters for the infrared (IR) pulse are identical to Fig. 6 except that the pump-probe delay is ∼17 fs. The intensities of the four nuclear wave packets are magnified by 40, 6.25, 6.25, and 71.4, respectively.

a.u. Thus, we are aware that it takes the nuclear wave packet along the $1^1\Pi_g$ curve ∼17 fs to move from the Franck-Condon region at around $R = 2.1$ a.u. to the internuclear positions of $R = 3$ a.u. To verify this speculation, we show the evolution of the nuclear wave packets along the $1^1\Pi_u$ and $1^1\Pi_g$ curves in Figs. 7(a) and 7(b) for a trajectory that dominates the variations of the 11.5- and 10-eV peaks in the nuclear KER spectrum at ∼17 fs in Fig. 6(a). The parameters for the selected trajectory are as follows: $t_1 = 83$ a.u., $t_2 = 99$ a.u., and $1^1\Pi_g$ as the initial state in N_2^{++}. It is clear that the nuclear wave packet first evolves along the $1^1\Pi_g$ curve to larger internuclear distances, and then the delayed IR pulse comes and induces a large dipole transition from the $1^1\Pi_g$ state to the $1^1\Pi_u$ state at around $R = 3$ a.u., leaving the nuclear wave packet eventually evolving along the $1^1\Pi_u$ curve.

In Fig. 6(a), we also notice that the peaks at ∼9 eV become more pronounced, and the peaks at ∼7.5 eV become less pronounced in the nuclear KER spectra for delays ∼17 fs. The change of these peaks have the same origin as the similar structure in Fig. 5. More importantly, this delay-dependent structure manifests that it also takes ∼17 fs for the nuclear wave packets in the $1^1\Pi_u$ state to move from the Franck-Condon region to the one-photon resonance region at around $R = 3$ a.u. One can similarly confirm this speculation by using Figs. 7(c) and 7(d) to show the evolution of the nuclear wave packets along the $1^1\Pi_u$ and $1^1\Pi_g$ curves for a selected dominant trajectory with $t_1 = 83$ a.u., $t_2 = 99$ a.u., and $1^1\Pi_u$ as the initial state in N_2^{++}. We also present the total yield of the fragmented N_2^{++} for delays between 0 and 60 fs in Fig. 6(c) by integrating the individual spectra in Fig. 6(a) with all the KER values. It is clear that the yield of fragmented N_2^{++} generally increases when the delay increases. This trend is consistent with the results in Refs. [32–34], where an decrease of the yield of the unfragmented N_2^{++} for increasing delays was reported. A further analysis of the time-resolved nuclear KER spectra can help to uncover the other nuclear dynamics involved.

V. CONCLUSIONS

In this paper, we investigate the ultrafast nuclear dynamics following inner-shell photoionization of N_2 in different pulse settings by using the MCWP method. We have obtained the nuclear KER spectra of N_2^{++} from the nondissociative states that support sharp vibrational resonances by using two spectral methods. We have discussed the origins of the peaks in the spectrum of N_2 interacting with a single x-ray pulse: The peaks at ∼7.3 and 7.8 eV come from tunneling of the barriers of the potential energy curves for the nondissociative states of $1^1\Pi_u$ and $2^1\Sigma_g^+$; the peak at ∼8.2 eV comes from over the barrier dissociation of the $2^1\Sigma_g^+$ curve; and the peak at ∼11.5 eV comes from direct dissociation along the $1^1\Pi_g$ curve. In addition to N_2 interacting with a single x-ray pulse, we apply an x-ray-pump–IR-probe setup to study the influence of the optical parameters of the IR pulses on the nuclear dynamics in N_2^{++}. The IR pulses couple the states in N_2^{++} together and thus open the possibility of controlling the ultrafast nuclear dynamics by adjusting the optical parameters of the IR pulses. From the nuclear KER spectra for six selected IR pulses, we see suppression of the signals peaking at ∼7.5 and 11.5 eV and an enhancement of the signals peaking at ∼9 and 10 eV for IR pulses with larger peak intensities or longer pulse durations. We find that the enhanced transition between the $1^1\Pi_u$ and $1^1\Pi_g$ states near the one-photon resonance positions

accounts for the suppression of the KER spectral signal peaking at ∼11.5 eV (7.5 eV) and the enhancement of the signal peaking at ∼10 eV (9 eV). Finally, we use the time-resolved nuclear KER spectra to extract the nuclear dynamics involved. We can see it takes ∼17 fs for the nuclear wave packets in the $1^1\Pi_g$ and $1^1\Pi_u$ states to move from the Franck-Condon region to the internuclear distances at around $R = 3$ a.u.

The results obtained in this paper show that the two spectral methods are useful in obtaining the nuclear KER spectrum for molecular dications and can be applied to investigate the nuclear dynamics involved in double ionization of other multielectron diatomic molecules.

ACKNOWLEDGMENTS

We thank Chuan Yu for very helpful suggestions and discussions. This paper was financially supported by the National Natural Science Foundation of China under Grants No. 12104189, No. 12104190, and No. 11947110, Natural Science Foundation of Jiangsu Province BK20210874 and General Project of Natural Science research in Colleges and Universities of Jiangsu Province (Grant No. 20KJB14008). Q.J. was also supported by the Scientific Research Foundation of Jiangsu University of Science and Technology (Grant No. 1052931901) and Jiangsu Province Innovative and Entrepreneurial Doctoral Fund 2020 (Grant No. 1054902004). P.X. was supported by the Scientific Research Foundation of Nanjing University of Posts and Telecommunications (Grant No. NY218097) and the Young Fund of Jiangsu Natural Science Foundation of China (Grant No. BK20180750). We also acknowledge support from the Young Fund of Jiangsu Natural Science Foundation of China (Grants No. BK20190953 and No. BK20190954).

[1] E. Gagnon, P. Ranitovic, X.-M. Tong, C. L. Cocke, M. M. Murnane, H. C. Kapteyn, and A. S. Sandhu, Soft x-ray-driven femtosecond molecular dynamics, Science **317**, 1374 (2007).

[2] M. S. Schöffler, J. Titze, N. Petridis, T. Jahnke, K. Cole, L. P. H. Schmidt, A. Czasch, D. Akoury, O. Jagutzki, J. B. Williams *et al.*, Ultrafast probing of core hole localization in N_2, Science **320**, 920 (2008).

[3] M. Lein, T. Kreibich, E. K. U. Gross, and V. Engel, Strong-field ionization dynamics of a model H_2 molecule, Phys. Rev. A **65**, 033403 (2002).

[4] G. N. Gibson, M. Li, C. Guo, and J. Neira, Strong-field dissociation and ionization of H_2^+ using ultrashort laser pulses, Phys. Rev. Lett. **79**, 2022 (1997).

[5] A. Palacios, J. L. Sanz-Vicario, and F. Martín, Theoretical methods for attosecond electron and nuclear dynamics: Applications to the H_2 molecule, J. Phys. B: At., Mol. Opt. Phys. **48**, 242001 (2015).

[6] S. De, I. A. Bocharova, M. Magrakvelidze, D. Ray, W. Cao, B. Bergues, U. Thumm, M. F. Kling, I. V. Litvinyuk, and C. L. Cocke, Tracking nuclear wave-packet dynamics in molecular oxygen ions with few-cycle infrared laser pulses, Phys. Rev. A **82**, 013408 (2010).

[7] W. Siu, F. Kelkensberg, G. Gademann, A. Rouzée, P. Johnsson, D. Dowek, M. Lucchini, F. Calegari, U. De Giovannini, A. Rubio *et al.*, Attosecond control of dissociative ionization of O_2 molecules, Phys. Rev. A **84**, 063412 (2011).

[8] J. N. Bull, J. W. L. Lee, and C. Vallance, Electron ionization dynamics of N_2 and O_2 molecules: Velocity-map imaging, Phys. Rev. A **91**, 022704 (2015).

[9] B. Zhang, J. Yuan, and Z. Zhao, Dynamic Core Polarization in Strong-Field Ionization of CO Molecules, Phys. Rev. Lett. **111**, 163001 (2013).

[10] X. Li, J. Yu, H. Xu, X. Yu, Y. Yang, Z. Wang, P. Ma, C. Wang, F. Guo, Y. Yang *et al.*, Multiorbital and excitation effects on dissociative double ionization of CO molecules in strong circularly polarized laser fields, Phys. Rev. A **100**, 013415 (2019).

[11] M. Abu-samha and L. B. Madsen, Effect of multielectron polarization in the strong-field ionization of the oriented CO molecule, Phys. Rev. A **101**, 013433 (2020).

[12] H. Gao, Y. Song, W. M. Jackson, and C. Y. Ng, Communication: State-to-state photodissociation study by the two-color VUV-VUV laser pump-probe time-slice velocity-map-imaging-photoion method, J. Chem. Phys. **138**, 191102 (2013).

[13] Q. Song, P. Lu, X. Gong, Q. Ji, K. Lin, W. Zhang, J. Ma, H. Zeng, and J. Wu, Dissociative double ionization of CO in orthogonal two-color laser fields, Phys. Rev. A **95**, 013406 (2017).

[14] A. Fischer, A. Sperl, P. Cörlin, M. Schönwald, H. Rietz, A. Palacios, A. González-Castrillo, F. Martín, T. Pfeifer, J. Ullrich *et al.*, Electron Localization Involving Doubly Excited States in Broadband Extreme Ultraviolet Ionization of H_2, Phys. Rev. Lett. **110**, 213002 (2013).

[15] A. Lafosse, M. Lebech, J. C. Brenot, P. M. Guyon, L. Spielberger, O. Jagutzki, J. C. Houver, and D. Dowek, Molecular frame photoelectron angular distributions in dissociative photoionization of H_2 in the region of the Q1 and Q2 doubly excited states, J. Phys. B: At., Mol. Opt. Phys. **36**, 4683 (2003).

[16] M. Lucchini, K. Kim, F. Calegari, F. Kelkensberg, W. Siu, G. Sansone, M. J. J. Vrakking, M. Hochlaf, and M. Nisoli, Autoionization and ultrafast relaxation dynamics of highly excited states in N_2, Phys. Rev. A **86**, 043404 (2012).

[17] M. Eckstein, C.-H. Yang, M. Kubin, F. Frassetto, L. Poletto, H.-H. Ritze, M. J. Vrakking, and O. Kornilov, Dynamics of N_2 dissociation upon inner-valence ionization by wavelength-selected XUV pulses, J. Phys. Chem. Lett. **6**, 419 (2015).

[18] M. Coville and T. D. Thomas, Molecular effects on inner-shell lifetimes: Possible test of the one-center model of Auger decay, Phys. Rev. A **43**, 6053 (1991).

[19] J. H. D. Eland, M. Tashiro, P. Linusson, M. Ehara, K. Ueda, and R. Feifel, Double Core Hole Creation and Subsequent Auger Decay in NH_3 and CH_4 molecules, Phys. Rev. Lett. **105**, 213005 (2010).

[20] O. Travnikova, J.-C. Liu, A. Lindblad, C. Nicolas, J. Söderström, V. Kimberg, F. Gel'mukhanov, and C. Miron, Circularly Polarized X Rays: Another Probe of Ultrafast Molecular Decay Dynamics, Phys. Rev. Lett. **105**, 233001 (2010).

[21] L. Fang, T. Osipov, B. Murphy, F. Tarantelli, E. Kukk, J. P. Cryan, M. Glownia, P. H. Bucksbaum, R. N. Coffee, M. Chen *et al.*, Multiphoton Ionization as a Clock to Reveal Molecular

Dynamics with Intense Short X-Ray Free Electron Laser Pulses, Phys. Rev. Lett. **109**, 263001 (2012).

[22] Z. Vager, R. Naaman, and E. P. Kanter, Coulomb explosion imaging of small molecules, Science **244**, 426 (1989).

[23] F. Légaré, K. F. Lee, I. V. Litvinyuk, P. W. Dooley, S. S. Wesolowski, P. R. Bunker, P. Dombi, F. Krausz, A. D. Bandrauk, D. M. Villeneuve *et al.*, Laser Coulomb-explosion imaging of small molecules, Phys. Rev. A **71**, 013415 (2005).

[24] I. A. Bocharova, A. S. Alnaser, U. Thumm, T. Niederhausen, D. Ray, C. L. Cocke, and I. V. Litvinyuk, Time-resolved Coulomb-explosion imaging of nuclear wave-packet dynamics induced in diatomic molecules by intense few-cycle laser pulses, Phys. Rev. A **83**, 013417 (2011).

[25] M. Magrakvelidze, O. Herrwerth, Y. H. Jiang, A. Rudenko, M. Kurka, L. Foucar, K. U. Kühnel, M. Kübel, N. G. Johnson, C. D. Schröter *et al.*, Tracing nuclear-wave-packet dynamics in singly and doubly charged states of N_2 and O_2 with XUV-pump–XUV-probe experiments, Phys. Rev. A **86**, 013415 (2012).

[26] C. Guo, M. Li, J. P. Nibarger, and G. N. Gibson, Single and double ionization of diatomic molecules in strong laser fields, Phys. Rev. A **58**, R4271 (1998).

[27] C. Guo and G. N. Gibson, Ellipticity effects on single and double ionization of diatomic molecules in strong laser fields, Phys. Rev. A **63**, 040701(R) (2001).

[28] E. Eremina, X. Liu, H. Rottke, W. Sandner, M. G. Schätzel, A. Dreischuh, G. G. Paulus, H. Walther, R. Moshammer, and J. Ullrich, Influence of Molecular Structure on Double Ionization of N_2 and O_2 by High Intensity Ultrashort Laser Pulses, Phys. Rev. Lett. **92**, 173001 (2004).

[29] C. S. Lehmann, A. Picón, C. Bostedt, A. Rudenko, A. Marinelli, D. Moonshiram, T. Osipov, D. Rolles, N. Berrah, C. Bomme *et al.*, Ultrafast x-ray-induced nuclear dynamics in diatomic molecules using femtosecond x-ray-pump–x-ray-probe spectroscopy, Phys. Rev. A **94**, 013426 (2016).

[30] A. Trabattoni, M. Klinker, J. González-Vázquez, C. Liu, G. Sansone, R. Linguerri, M. Hochlaf, J. Klei, M. J. J. Vrakking, F. Martín *et al.*, Mapping the Dissociative Ionization Dynamics of Molecular Nitrogen with Attosecond Time Resolution, Phys. Rev. X **5**, 041053 (2015).

[31] A. M. Hanna, O. Vendrell, and R. Santra, Time-resolved x-ray/optical pump-probe simulations on N_2 molecules, Struct. Dyn. **6**, 024101 (2019).

[32] J. M. Glownia, J. Cryan, J. Andreasson, A. Belkacem, N. Berrah, C. I. Blaga, C. Bostedt, J. Bozek, L. F. DiMauro, L. Fang *et al.*, Time-resolved pump-probe experiments at the LCLS, Opt. Express **18**, 17620 (2010).

[33] A. M. Hanna, O. Vendrell, A. Ourmazd, and R. Santra, Laser control over the ultrafast coulomb explosion of N_2^{2+} after Auger decay: A quantum-dynamics investigation, Phys. Rev. A **95**, 043419 (2017).

[34] M. K. Ganesa Subramanian, R. Santra, and R. Welsch, Infrared-laser-pulse-enhanced ultrafast fragmentation of N_2^{2+} following Auger decay: Mixed quantum-classical simulations, Phys. Rev. A **98**, 063421 (2018).

[35] E. Baldit, S. Saugout, and C. Cornaggia, Coulomb explosion of N_2 using intense 10- and 40-fs laser pulses, Phys. Rev. A **71**, 021403(R) (2005).

[36] R. N. Coffee, L. Fang, and G. N. Gibson, Light-induced potentials ignite dissociation of N_2^{2+}, Phys. Rev. A **73**, 043417 (2006).

[37] W. Lai, L. Pei, and C. Guo, Dissociation of doubly and triply charged N_2 in strong laser fields, Phys. Rev. A **84**, 043413 (2011).

[38] H. Iwayama, T. Kaneyasu, Y. Hikosaka, and E. Shigemasa, Stability and dissociation dynamics of N_2^{++} ions following core ionization studied by an Auger-electronphotoion coincidence method, J. Chem. Phys. **145**, 034305 (2016).

[39] H. A. Leth, L. B. Madsen, and K. Mølmer, Monte Carlo Wave Packet Theory of Dissociative Double Ionization, Phys. Rev. Lett. **103**, 183601 (2009).

[40] H. A. Leth, L. B. Madsen, and K. Mølmer, Monte Carlo wave packet approach to dissociative multiple ionization in diatomic molecules, Phys. Rev. A **81**, 053409 (2010).

[41] H. A. Leth, L. B. Madsen, and K. Mølmer, Dissociative double ionization of H_2 and D_2: Comparison between experiment and Monte Carlo wave packet calculations, Phys. Rev. A **81**, 053410 (2010).

[42] Q. Jing and L. B. Madsen, Laser-induced dissociative ionization of H_2 from the near-infrared to the mid-infrared regime, Phys. Rev. A **94**, 063402 (2016).

[43] Q. Jing, R. Y. Bello, F. Martín, A. Palacios, and L. B. Madsen, Monte Carlo wave-packet approach to trace nuclear dynamics in molecular excited states by XUV-pump–IR-probe spectroscopy, Phys. Rev. A **97**, 043426 (2018).

[44] H. A. Leth and L. B. Madsen, Dissociative multiple ionization of diatomic molecules by extreme-ultraviolet free-electron-laser pulses, Phys. Rev. A **83**, 063415 (2011).

[45] J. P. Cryan, J. M. Glownia, J. Andreasson, A. Belkacem, N. Berrah, C. I. Blaga, C. Bostedt, J. Bozek, N. A. Cherepkov, L. F. DiMauro *et al.*, Molecular frame Auger electron energy spectrum from N_2, J. Phys. B: At., Mol. Opt. Phys. **45**, 055601 (2012).

[46] B. Kempgens, A. Kivimäki, M. Neeb, H. M. Köppe, A. Bradshaw, and J. Feldhaus, A high-resolution N 1*s* photoionization study of the N_2 molecule in the near-threshold region, J. Phys. B: At. Mol. Opt. Phys. **29**, 5389 (1996).

[47] M. D. Feit, Jr., J. Fleck, and A. Steiger, Solution of the Schrödinger equation by a spectral method, J. Comput. Phys. **47**, 412 (1982).

[48] H. A. Leth, Dissociative Ionization—A Study Using the Monte Carlo Wave Packet Approach, Ph.D. thesis, Aarhus University, 2011.

[49] M. Kato, Y. Morishita, M. Oura, H. Yamaoka, Y. Tamenori, K. Okada, T. Matsudo, T. Gejo, I. Suzuki, and N. Saito, Absolute photoionization cross sections with ultra-high energy resolution for Ar, Kr, Xe and N_2 in inner-shell ionization regions, J. Electron. Spectrosc. Relat. Phenom. **160**, 39 (2007).